

https://dspace.org/

Nitrogendoped porous biocarbon materials originated from heavy biooil and their CO2 adsorption characteristics

J Tang; B Li; Yusuf Isa; X Xie; A Kozlov ...

https://hdl.handle.net/10539/43430
WOS

Downloaded from a DSpace repository. https://dspace.org/

Biomass and Bioenergy 182 (2024) 107113

Contents lists available at ScienceDirect

Biomass and Bioenergy

journal homepage: www.elsevier.com/locate/biombioe

Nitrogen-doped porous biocarbon materials originated from heavy bio-oil and their CO_2 adsorption characteristics

Jiazhen Tang [a], Bin Li [a,b,*], Yusuf Makarfi Isa [c], Xing Xie [a,**], Alexander Kozlov [d], Maxim Penzik [d], Dongjing Liu [a]

[a] School of Energy and Power Engineering, Jiangsu University, Zhenjiang, 212013, China
[b] School of Engineering, Anhui Agricultural University, Hefei, 230036, China
[c] School of Chemical and Metallurgical Engineering, University of the Witwatersrand, Johannesburg, 2050, South Africa
[d] Melentiev Energy Systems Institute SB RAS, 130 Lermontov Street, Irkutsk, 664033, Russia

ARTICLE INFO

Keywords:
N-doping
KOH activation
Porous biocarbon materials
CO_2 adsorption
Biocoke
Heavy bio-oil

ABSTRACT

To realize the high-value utilization of biocoke derived from heavy bio-oil, N-doped porous biocarbon materials were prepared through co-pyrolysis of biocoke with urea and KOH activation, and their physiochemical structures and CO_2 adsorption capacity were analyzed. Compared with direct heat treatment of biocoke at 550 °C, N-doping at the same temperature would reduce the biocarbon yield and block its pores, but the pore structure could be recovered through further heating to 800 °C. KOH activation at 800 °C could produce highly porous biocarbon materials with BET surface areas of 1710.20–3361.45 m^2/g in the expense of yield reduction. The mass ratio of KOH to biocarbon material significantly affect its pore formation and distribution. Moderate activation (ratio of 2, 550NBC-800-2) could generate more micropores, over activation (ratio of 3 and 4, 550NBC-800-3/4) could further increased its total surface area, but resulted in the damage/merging of micropores to mesopores. KOH activation was found to increase the O-containing groups and decrease the large ring systems in the biocarbon as well, but the etching of KOH would lead to the releasing of N previously existed/doped in the biocarbon. The CO_2 adsorption performance of the biocarbon material was closely related to its pore structure and surface N-doping. At a high CO_2 pressure (1 bar), the CO_2 adsorption capacity of biocarbon materials was more dependent on its micropore areas. But at a low CO_2 pressure (0.15 bar), N-doping, especially to form more N-5 in biocarbon, was observed to be more important than its micropores.

1. Introduction

Bio-oil is an important liquid product from biomass pyrolysis. It is complex organic mixture, which contains a wide range of organic substances, such as carboxylic acids, aldehydes, ketones, furans, phenolics and anhydrosugars, etc. [1–4]. Despite of its significantly higher volumetric energy density compared with biomass, the raw bio-oil is a kind of acidic and highly oxygenated liquid with a heat value of around only 15 MJ/kg, upgrading is thus required for its high-value utilization [5,6]. Distillation and hydrodeoxygenation are two common ways that people currently use for bio-oil upgrading [7–10]. Unfortunately, these processes always suffer from the severe coking problem due to the thermally unstable nature of the bio-oil [11–16]. The high content of oxygen-containing organic compounds would be easily polymerized once heating the bio-oil [17,18], while most of the upgrading processes require to be heated.

The formation of coke during bio-oil upgrading would foul/block the pipeline and/or reactor, deactivate the catalyst, reduce the process efficiency, and endanger the system operation. A lot of efforts have been made to alleviate the coke formation during bio-oil upgrading, including stabilization of bio-oil by adding alcohols during esterification [19], division of hydrodeoxygenation into multiple temperature stages [20,21], and modification of catalyst during cracking [22,23], etc. However, up to now, the coke formation still cannot be eliminated and is remained as a main challenge to hinder the development of bio-oil upgrading technologies [24]. In our recent study, we have proposed a new strategy for bio-oil utilization [25]. Instead of alleviating the coke formation, bio-oil will be firstly heat treated to coke the high coking tendency

* Corresponding author. School of Energy and Power Engineering, Jiangsu University, Zhenjiang, 212013, China.
** Corresponding author.
E-mail addresses: libin198520@126.com (B. Li), xiexing_xx@126.com (X. Xie).

https://doi.org/10.1016/j.biombioe.2024.107113
Received 1 January 2024; Received in revised form 11 February 2024; Accepted 12 February 2024
Available online 17 February 2024
0961-9534/© 2024 Elsevier Ltd. All rights reserved.

compounds, while the low coking tendency compounds will be evaporated out for further upgrading without coking issue. The biocoke formed during the heat treatment with a yield of around 17 wt% at 350 °C is an almost ash-free and highly carbonaceous material, how to realize its high-value utilization would significantly affect the efficiency and economy of the entire process.

In recent years, carbon neutrality is a hot topic and has attracted increasing attentions globally. Direct capturing CO_2 from large point sources is regarded as an effective way to mitigate the CO_2 emission [26]. Porous carbon materials, with the advantages of high adsorption capacity, fast kinetics, high thermal/chemical stability, and easy regeneration, is one of the most promising materials for efficient CO_2 adsorption [25,27]. However, the original biocoke for heat treatment of bio-oil has rare pores [25], it must be activated before it can be used as a CO_2 adsorbent. As a new source of carbon, the interactions between biocoke and activator and the resulted pore formation and distribution are still unclear, which would largely affect the CO_2 adsorption performance. Meanwhile, it has been reported that N-doping can increase the surface basicity of the carbon materials, thus improve its surface infinity to CO_2 molecules [28–30]. The pore structure and N-doping both play important roles for carbon materials during CO_2 adsorption, but to which extent each of them plays remains unclear.

Therefore, in this study, biocoke, as a new carbonaceous material derived from heat treatment of heavy bio-oil, was subjected to modification to seek for high-value utilization. KOH activation and N-doping were both applied to get a N-doped porous biocarbon material for CO_2 adsorption. Different biocarbon materials from direct heat treatment/N-doping, KOH activation and their combinations were prepared for comparison. The physical and chemical structures of the biocarbon materials as well as their CO_2 adsorption capacities were analyzed in-depth. The results obtained from this study would gain a better understanding on the effects of pore structure and N-doping on the CO_2 adsorption characteristics. It could not only provide a good way for the high-value utilization of this heavy oil derived biocoke, but also support the cascade utilization and upgrading of bio-oil.

2. Experimental

2.1. Heavy bio-oil

The heavy bio-oil was obtained from Hubei Bluefire Ecological Energy Co., Ltd. It was produced by a 1 t/h moving-bed biomass pyrolysis plant with a peak temperature of around 600 °C and bamboo as feedstock. The initial bio-oil includes both light phase and heavy phase, while only the heavy phase bio-oil was used in this study. It has a dark brown color with a big smell, it is a very viscous (heavy) liquid.

2.2. Biocoke production from heat treatment of heavy bio-oil

The biocoke is the precursor to produce N-doped porous biocarbon materials. It was prepared by the heat treatment of heavy bio-oil in a tube furnace under N_2 atmosphere at 350 °C for 2 h, the detailed procedure could be found elsewhere [25]. Briefly, around 4 g of heavy bio-oil loaded in a ceramic boat with a closed cap was positioned in a tube furnace, it was then heated from room temperature to 350 °C with 10 °C/min in a N_2 flow of 100 mL/min, and kept isothermal for 120 min. The solid residue inside the boat after heat treatment is the so-called biocoke (denoted as "BC"). The yield of biocoke is 16.91 ± 0.57 wt%, with an elemental composition of 81.56 wt% of C, 4.89 wt% of H, 1.04 wt% of N, 0.44 wt% of S and 12.09 wt% of O (by difference).

2.3. N-doped porous biocarbon materials production

The preparation of N-doped porous biocarbon materials mainly includes two steps: N-doping and biocarbon activation. For N-doping process, analytical purity of urea purchased from Sinopharm Chemical Reagent Co., Ltd (Shanghai, China) was chosen as the N source. It was well mixed with biocoke using a ceramic mortar with a mass ratio of 1:1. The resulted mixture was then heat treated in a tube furnace at 550 °C with a heating rate of 5 °C/min and kept isothermal for 180 min [31]. The solid residue left after this co-pyrolysis process was the expected N-doped biocarbon material. It was then cooled down and collected for further use. The obtained N-doped biocarbon material is denoted as "550NBC", where, "550" represents the heat treatment temperature, and "N" represents the N-doping. A biocarbon sample prepared at the same condition but without urea addition was also made for comparison, which was denoted as "550BC".

For biocarbon activation process, analytical purity of KOH purchased from Sinopharm Chemical Reagent Co., Ltd (Shanghai, China) as well was used for the chemical activation of the biocarbon material to produce more porous structures. The detailed procedure was described as follows: Firstly, around 1.3 g of biocarbon was well mixed with KOH in a mortar according to the certain ratios (mass ratio of KOH/biocarbon of 2, 3 and 4), then the resulted mixture was put inside a nickel boat and positioned in a horizontal tube furnace for activation. It was heated to 800 °C at the rate of 5 °C/min in a 100 mL/min N_2 atmosphere, and maintained isothermal for 120 min. After activation, the sample was cooled down and then washed with 1 mol/L HCl solution to remove the K-containing species, it was then washed with deionized water until neutral and dried at 105 °C for 6 h to get the final porous biocarbon materials. They are denoted as "Biocarbon-800-X", here, "800" represents the activation temperature, and "X" represents the mass ratio of KOH to biocarbon. It should be noted that different biocarbon samples were activated in the study, including BC, 550BC and 550NBC. Hence, the "Biocarbon" in "Biocarbon-800-X" could be BC, 550BC and 550NBC as well.

Generally, the biocarbon was firstly doped with N, and then it was activated with KOH. For comparison, some of the samples were only doped with N or just activated, such as 550NBC, BC-800-3 and 550BC-800-3. Some of the samples were only heat treated without activation, e.g., 550NBC-800-0. In addition, a sample (550BC) firstly activated with KOH and then doped with N was also made for comparison, it is denoted as "550BC-800-3-550 N".

2.4. Characterization of biocarbon materials

The physical pore structure of the biocarbon materials was determined with an Accelerated Surface Area and Porosity Tester (Micromeritics, ASAP 2420) through N_2 adsorption-desorption at 77K. All the samples were degassed at 250 °C for 6 h before the test. Electron scanning microscope (SEM, Zeiss Supra 55) was performed to observe the micromorphology of the biocarbon with the magnification of 5000 and 20000 times.

The elemental composition (CHNS) of the biocarbon materials were tested with an Elemental Analyzer (Vario EL III). The surface chemical structure of the biocarbon was characterized by X-ray photoelectron spectroscopy (XPS). A Thermo Fisher Scientific K-Alpha Spectrometer equipped with monochromatic Al Kα X-ray was used to record to the survey spectrum and the high-resolution spectra of C1s and N1s. The carbon skeleton of the biocarbon was analyzed with Renishaw InVia Raman spectrometer with an Ar + laser (532 nm) in the scanning spectrum range of 4000-400 cm^{-1}.

The biocarbon materials obtained in the study were finally subjected to the CO_2 adsorption test to evaluate the relationship between their structures and CO_2 adsorption performance. It was carried out on an Automatic Specific Surface Porosity Analyzer (Micromeritics, ASAP2460). The CO_2 isothermal adsorption curves of the biocarbon materials were measured at 25 °C each time. To improve the accuracies during the test, all the samples were degassed at 200 °C for 6 h in advance to remove impurities in the pores.

3. Results and discussion

3.1. Yields of biocarbon materials

Yield is an important consideration during the production of biocarbon materials. It not only affects its mass production, but also is relevant to the formation mechanism. Fig. 1 shows the mass yields of biocarbon materials through different heat treatment methods including activation, N-doping and direct heat treatment. The yields of biocarbon materials are on a basis of biocoke (BC) obtained from heat treatment of heavy bio-oil at 350 °C for 120 min.

From Fig. 1, it can be found that significant weight loss was observed for the biocarbon after heat treated at 550 °C (550BC) due to more volatiles being released, as the original biocoke was generated at 350 °C. When biocoke was co-pyrolyzed with urea (N-doping), the final yield of 550NBC (68.70 wt%) was even lower than that of 550BC (73.90 wt%) despite of the additional N doping onto biocarbon, the addition of urea would promote the decomposition of biocoke resulting in a lower yield. Further heating 550NBC to 800 °C (550NBC-800-0) would cause more sufficient volatiles releasing, a lower yield of 60.46 wt% was obtained.

KOH activation at 800 °C was also performed with different mass ratios of KOH to biocarbon as shown in Fig. 1. The etching of KOH to biocarbon resulted in an obvious reduced yield of activated biocarbon compared with that of purely thermal cracking (550NBC-800-0). With the mass ratio of KOH to biocarbon (550NBC) increasing from 2 to 4, the yield of activated biocarbon decreased from 50.99 to 43.30 wt%. Similar result was also found for 550BC-800-3, without N-doping, the yield of activated biocarbon (43.01 wt%) was just slightly lower. Further doping N on the activated biocarbon (550BC-800-3-550 N) would again decrease its yield, which is consistent with the previous result. In addition, it can be also found from Fig. 1 that, two-steps of heat treatment/N-doping and activation would yield more biocarbon materials than one-step direct activation (BC-800-3, 36.93 wt%), it might be a good guidance for the mass production of biocarbon materials as well.

3.2. Surface morphology and porous structure of biocarbon materials

The surface micromorphology of biocarbon materials were analyzed with SEM. Three selected samples (BC, BC-800-3 and 550NBC-800-3) were tested and are shown in Fig. 2 with two magnification times of 5000 and 20000. Significant differences could be found in the

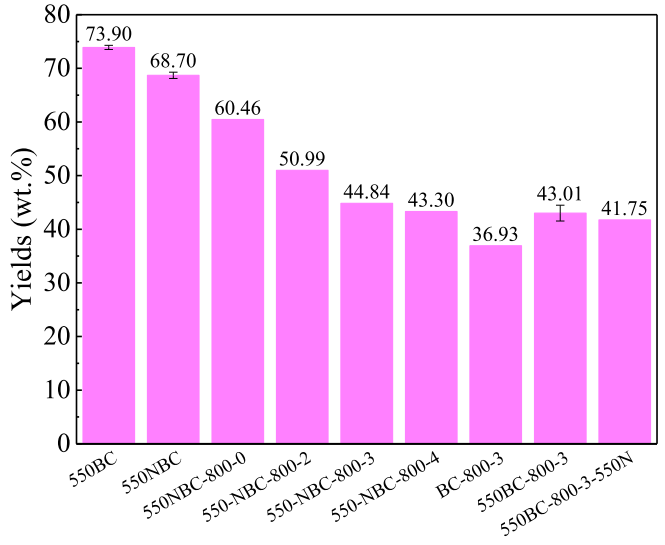


Fig. 1. Yields of biocarbon materials originated from heavy bio-oil (on a basis of biocoke (BC) obtained from heat treatment of heavy bio-oil at 350 °C for 120 min).

micromorphologies of the three samples. The original biocoke (BC) obtained from the heat treatment of heavy bio-oil showed a relative smooth surface with less porous structures, which might be due to the relatively lower heat treatment temperature of 350 °C. While after KOH activation at 800 °C, BC-800-3 exhibited large amount of porous structures on its surface, which would be surely good for its adsorption performance. As stated before, such pores were mainly from the volatiles releasing at high temperature and the etching effect of KOH during the activation process. Comparatively, the 550NBC-800-3 showed very different pore structures although it also went through the same activation process. The biocarbon precursor also significantly affected the pore formation of the biocarbon materials.

Table 1 summarizes the detailed porous characteristics of the biocarbon materials through the N_2 adsorption-desorption method. From the table, it can be observed that the original BC had almost no pores, it might be not suitable for other uses except as a fuel. Further treatment is thus required to improve its property. Direct heat treatment at 550 °C (550BC) significantly increased the porosity of the biocarbon due to the volatiles releasing generating some micropores (t-plot micropore area of 118.00 m^2/g), while N-doping would block the pore structures or destroy the formation of pore structures of the biocarbon (550NBC of 2.2 m^2/g) during the co-pyrolysis of BC and urea. Further treating 550NBC at 800 °C would generate more pores on the surface of 550NBC-800-0 (177.34 m^2/g), although the proportion of micropore area (160.45 m^2/g) was higher, its average pore size was still relatively bigger for CO_2 adsorption (4.50 nm). Further reduction in the pore size and increase in the micropore surface area would be needed for purpose of CO_2 adsorption.

KOH activation was thus introduced to create pores on the surface of the biocarbon materials. Compared with only heat treatment at 800 °C (550NBC-800-0), KOH activation significantly increased the specific surface area of the biocarbon materials, BET surface areas of around 1710.20–3361.45 m^2/g were achieved with the mass ratios of KOH to biocarbon of 2–4, and the pore size decreased sharply to 2.22–2.30 nm. Also, it can be found that at a low mass ratio of KOH to biocarbon of 2, the moderate activation would generate more micropores, with a high t-plot micropore area of 1257.65 m^2/g and a relatively lower t-plot external surface area of 452.55 m^2/g obtained. Further increasing the mass ratio of KOH to biocarbon would cause more severe activation/etching of the biocarbon structures, the micropores would be damaged or merged to form more mesopores, thus the micropore area decreased with the increase of external surface area (550NBC-800-3) [32–34]. When the mass ratio of KOH to biocarbon increased to 4, mainly external surface area was obtained for the biocarbon although the total BET surface area got a maximum value of 3361.45 m^2/g. The micropore volume showed similar trend with that of micropore area.

The porous structure of directly activated biocoke (BC-800-3) was also tested as shown in Table 1, it can be found that one step activation could achieve a high BET surface area as well although it was somehow lower than that of two-step biocarbon (550BC-800-3), but the micropore area and volume were significantly higher than those of two-step one. The pore structure of 550BC-800-3 was quite similar with that of 550NBC-800-3, while the later one had more micropores relatively. Further doping N on the activated biocarbon at 550 °C did not reduce the BET surface area of the biocarbon, but increased the micropore area and volume and decreased the external surface area.

The pore size distribution of biocarbon materials prepared under different conditions was also analyzed and is presented in Fig. 3. From the figure, it can be observed that KOH activation made the pore size distributions of different biocarbon materials were somehow similar, which was narrowed mainly within the range of 0.4–4 nm (micro- and meso-pores). For the N-doped activated biocarbon (Fig. 3a), as mentioned previously in Table 1, with lower mass ratio of KOH to biocarbon, the activated biocarbon (550NBC-800-2) showed more micropores with less mesopores, the pore size distribution further proved this conclusion. The micropores of the activated biocarbon mainly ranged in

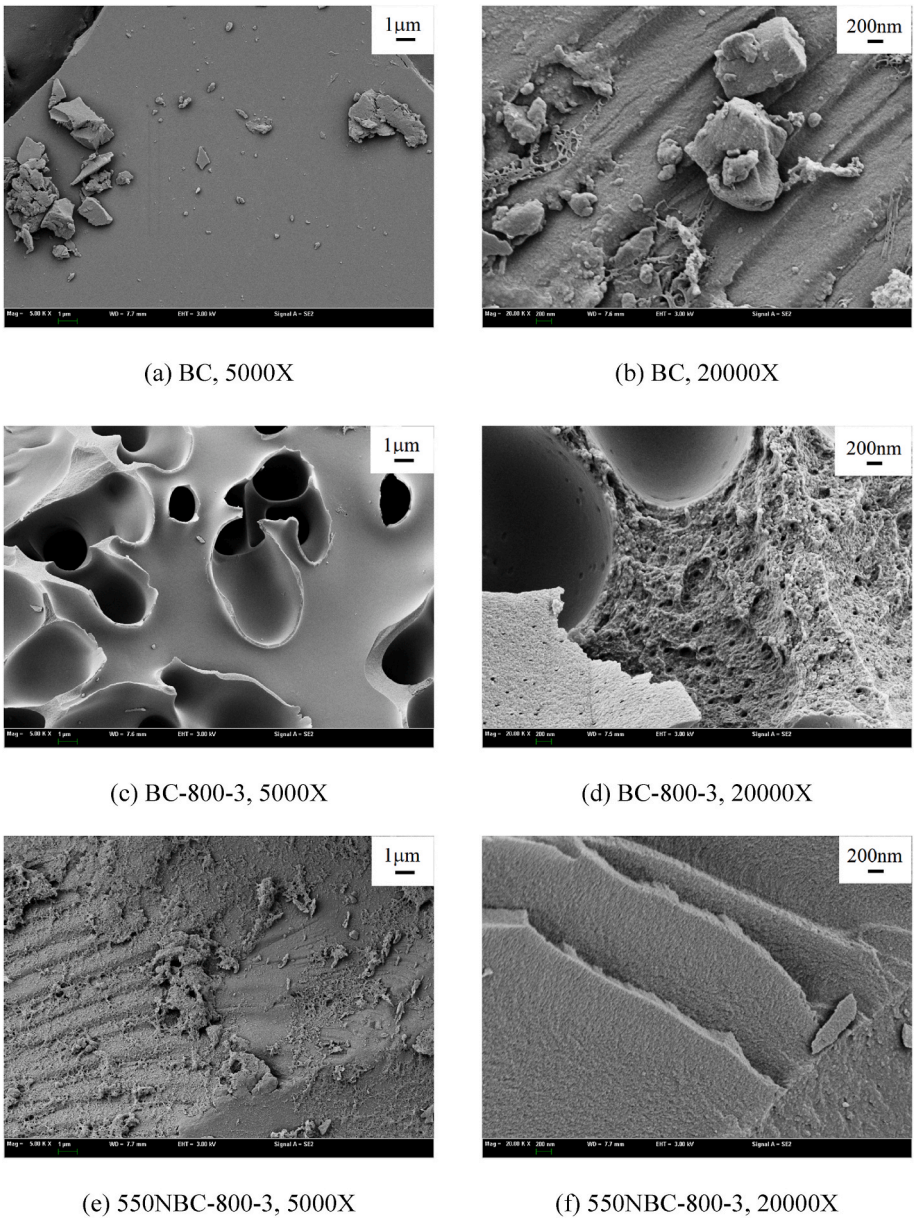


Fig. 2. SEM images of three biocarbon materials under different magnification times. a, b: BC, 5000-20000X; c, d: BC-800-3, 5000-20000X; e, f: 550NBC-800-3, 5000-20000X.

Table 1
Pore characteristics of biocarbon materials originated from heavy bio-oil.

Samples	BET surface area (m^2/g)	t-plot Micropore area (m^2/g)	t-plot External surface area (m^2/g)	Pore volume ($\times 10^{-2}$ mL/g)	t-plot Micropore volume ($\times 10^{-2}$ mL/g)	Pore size (nm)
BC	0.61	–	0.87	0.10	0.02	8.01
550BC	143.69	118.00	25.69	7.84	5.80	4.67
550NBC	2.20	0.55	1.65	1.01	0.03	33.15
550NBC-800-0	177.34	160.45	16.89	9.08	7.85	4.50
550NBC-800-2	1710.20	1257.65	452.55	89.83	66.81	2.24
550NBC-800-3	2601.78	736.03	1865.74	138.11	42.36	2.22
550NBC-800-4	3361.45	–	3539.91	179.79	14.73	2.30
BC-800-3	2133.70	954.99	1178.71	115.59	52.51	2.31
550BC-800-3	2575.01	622.21	1952.80	136.55	37.97	2.22
550BC-800-3-550 N	2581.48	929.21	1652.27	135.47	52.97	2.17

0.5–0.9 nm, 1.0–1.2 nm, and 1.5–2 nm, while the mesopores of the activated biocarbon were mainly ranged in 2–4 nm, the average pore size was around 2.22–2.30 nm (Table 1). With more KOH addition during the activation, the micropores reduced with more mesopores generated as shown in Fig. 3a. For the directly activated biocarbon (Fig. 3b), similar pore size distributions were observed with those of N-

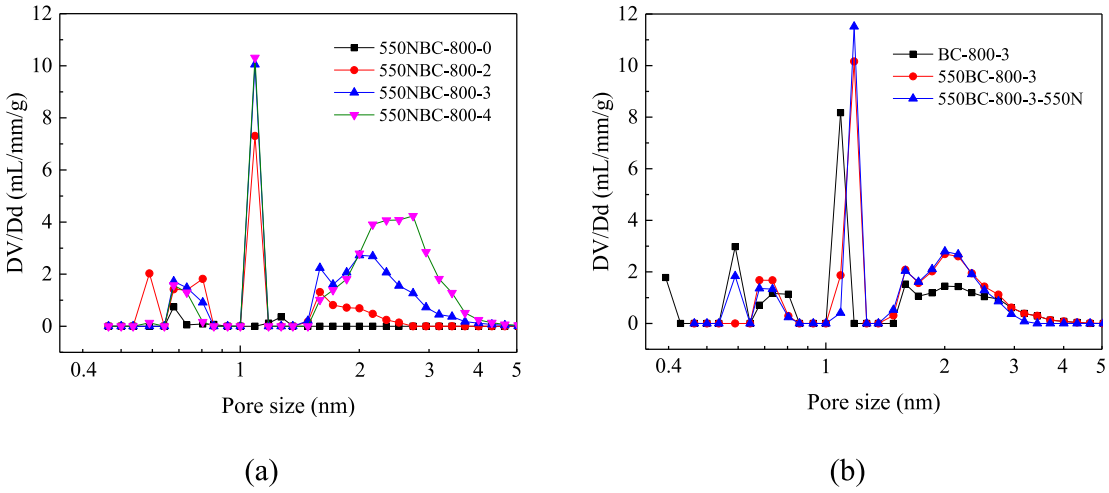


Fig. 3. DFT pore size distributions of heavy bio-oil derived biocarbon materials prepared under different conditions.

doping activated biocarbon (Fig. 3a). Also, BC-800-3 showed relatively smaller pore sizes than the two-step activated biocarbon (550BC-800-3). In addition, N-doping after KOH activation (550BC-800-3-550 N) would not significantly change the pore size distribution of the biocarbon.

3.3. Chemical composition and surface properties of biocarbon materials

The chemical composition of the biocarbon materials was tested and is summarized in Table 2. From the table, it can be found that the original BC was already a highly carbonaceous material with a C of 81.56 wt%, H of 4.89 wt%, and O of 12.09 wt%, the N content of BC was 1.04 wt%. Further heat treatment, N-doping and KOH activation all increased its carbonization degree with the increase of C content and the decrease of H and O contents. For instance, after heat treated at 550 °C, the C content of 550BC increased to 88.94 wt%, the H and O contents decreased to 2.76 wt% and 7.39 wt%, respectively. The N content in 550BC somehow concentrated due to the decreased mass yield. N-doping further increased the N content in the biocarbon from 1.37 wt% to 2.05 wt%, the H content increased slightly with O content decreasing. Further heating 550NBC to 800 °C, the carbonization degree of 550NBC-800-0 increased further as illustrated in the table, but the N content decreased slightly to 1.86 wt% due to the possible cracking/decomposition of thermally unstable N-containing species at high temperature.

From Table 1, it can be also observed that the N doped in biocarbon (550NBC) was subsequently released during the KOH activation process, the N contents of 550NBC-800-2, 3 and 4 were only of 0.07–0.28 wt%, which were largely lower than that of 550NBC. N seemed to be failed to dope in the activated biocarbon materials. The etching/activation of KOH to carbon structure would easily decompose/destroy the N species bonded in the biocarbon structure [5]. Similar results were also obtained for the one-step and two-step activation biocarbon materials (BC-800-3 and 550BC-800-3). To successfully dope the N on the biocarbon surface, the biocarbon was firstly activated and then doped with N, a N content of 1.2 wt% was finally obtained for 550BC-800-3-550 N.

Table 2
Elemental composition of biocarbon materials originated from heavy bio-oil.

Samples	Elemental composition (wt.%)				
	C	H	N	S	O[a]
BC	81.56	4.89	1.04	0.44	12.09
550BC	88.94	2.76	1.37	0	7.39
550NBC	88.22	3.13	2.05	0.09	6.53
550NBC-800-0	91.19	2.03	1.86	0.02	4.91
550NBC-800-2	92.66	1.42	0.07	0	5.86
550NBC-800-3	93.81	1.28	0.14	0	4.77
550NBC-800-4	93.88	1.01	0.28	0	4.85
BC-800-3	91.36	1.56	0.53	0	6.56
550BC-800-3	90.89	1.32	0.07	0.53	7.20
550BC-800-3-550 N	92.91	0.97	1.20	0.21	4.72

[a] Calculated by difference.

The carbon structure and surface functionalities of biocarbon materials originated from heavy bio-oil were analyzed with XPS spectrometry. All the spectra were corrected by positioning the primary peak of C1s to 284.4 eV to exclude the charging effects on binding energies during the test. The high resolution C1s and N1s spectra of the biocarbon materials were then deconvoluted by Avantage software to get the C-/O-/N-containing groups. For C1s spectra, 7 Gauss and Lorenz peaks assigned to C-C_{low} (283.44 ± 0.11 eV), C-$C_{primary}$ (284.27 ± 0.05 eV), C-C_{high} (284.93 ± 0.09 eV), C–O (286.03 ± 0.12 eV), C═O (286.85 ± 0.23 eV), COO (288.62 ± 0.17 eV) and pi-pi* (291.00 ± 0.00 eV) were applied to fit the curves [35,36]. Where, C-$C_{primary}$ represents the aromatic C–C/C–H bonds, C-C_{low} and C-C_{high} represent the disordered and/or defective carbon structures. C–O, C═O and COO represent the alcohol and ether C–O groups, the carbonyl groups, and the carboxyl, lactone and/or ester groups, respectively. While pi-pi* is the transition peak for primary C–C peak. For N1s spectra, 4 Gauss and Lorenz peaks assigned to N-6 (398.68 ± 0.18 eV), N-5 (399.97 ± 0.22 eV), N-Q (401.67 ± 0.18 eV), and N–O (403.34 ± 0.49 eV) were used to fit the curves [37]. Where, N-6, N-5, N-Q, and N–O represent the pyridinic N, pyrrolic N, graphitic N and N oxides, respectively. The representative deconvoluted C1s and N1s spectra of 550NBC are shown in Fig. 4.

To semi-quantitatively analyze the differences of varied biocarbon materials in the surface chemical structures, the deconvolution results of C1s and N1s were summarized and are presented in Table 3. From the table, it can be observed that all the biocarbon materials showed very similar aromatic C-$C_{primary}$ structure, further heat treating, N-doping and KOH activation would be more to affect their carbon defects (C-C_{low} and C-C_{high}) and surface O-/N-containing groups. It might be because of that biocarbon materials were all derived from heat treatment of heavy bio-oil rich in aromatic compounds, further treatments would not significantly increase their aromatic C–C/C–H structures. When heat treating at 550 °C, the defects (summary of C-C_{low} and C-C_{high}) in carbon structure decreased, more O-containing groups (C–O, C═O and COO) were observed on the biocarbon surface (550BC) despite of the fact of decreasing O content. Heat treatment might somehow concentrate the O-containing groups on the biocarbon surface. N-doping (550NBC) slightly increased the defects in carbon structure but decreased the O-containing groups. Further heating to 800 °C (550NBC-800-0), the O-

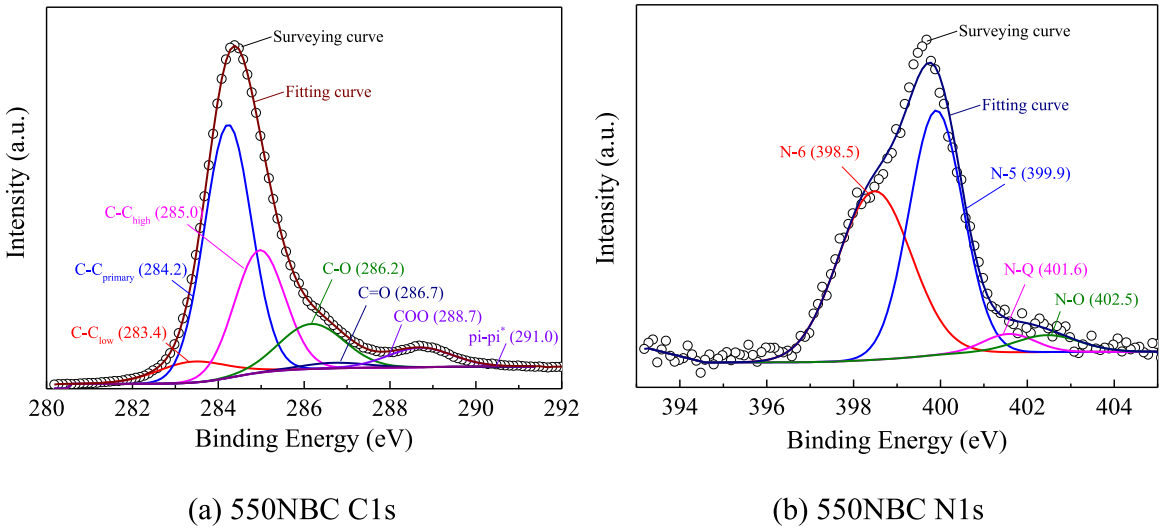


Fig. 4. Deconvolution of typical XPS spectra of biocarbon materials: (a) 550NBC C1s and (b) 550NBC N1s.

Table 3
XPS C1s and N1s deconvolution results of biocarbon materials obtained under different conditions.

Samples	C1s Spectra							N1s spectra			
	C-C$_{low}$	C-C$_{primary}$	C-C$_{high}$	C–O	C═O	COO	pi-pi*	N-6	N-5	N-Q	N–O
BC	6.15	49.02	30.39	9.51	1.97	2.76	0.21	20.53	64.91	9.25	5.31
550BC	6.18	49.74	23.52	13.99	0.82	5.69	0.06	35.19	54.28	7.49	3.04
550NBC	6.19	49.47	25.46	12.13	1.43	5.21	0.11	45.01	47.59	3.42	3.98
550NBC-800-0	5.72	49.49	26.68	8.78	4.56	4.59	0.16	23.01	60.29	14.47	2.23
550NBC-800-2	13.97	48.46	19.38	9.85	2.74	5.22	0.38	84.26	5.31	8.15	2.28
550NBC-800-3	6.21	45.58	21.47	18.94	0	7.63	0.18	50.79	44.58	3.04	1.59
550NBC-800-4	5.55	49.35	17.34	20.04	0	7.58	0.14	54.58	39.34	4.28	1.81
BC-800-3	5.87	43.33	26.06	17.03	0	7.45	0.26	48.17	42.01	6.29	3.53
550BC-800-3	5.12	49.82	19.08	14.45	5.36	6.08	0.07	15.35	74.32	4.8	5.53
550BC-800-3-550 N	5.53	45.58	25.08	15.79	0.06	7.78	0.19	42.95	46.39	7.97	2.7

containing groups decreased as its O content largely reduced. KOH activation also largely changed the chemical structure of biocarbon materials, generally resulted in decrease in carbon defects and increase in O-containing groups. For instance, compared BC with BC-800-3, the carbon defects decreased from 36.54% to 31.93%, while the O-containing groups increased from 14.24% to 24.48%. Similar trends could be also found for 550BC and 550BC-800-3, as well as 550NBC and 550NBC-800-3/4. While for the N1s deconvolution results, the original N in BC more existed as pyrrole nitrogen (N-5) of 64.91%, followed by pyridine nitrogen (N-6), quaternary nitrogen (N-Q) and nitrogen oxides (N–O). Upon heating (550BC), N-5 partially transformed to N-6, and the contents of N-Q and N–O decreased as well. While for N-doping by co-heating of biocarbon with urea, more N-6 was introduced into the resulted biocarbon materials (550NBC and 550BC-800-3-550 N). Further heating 550NBC to 800 °C (550NBC-800-0), part of the N-6 transformed to N-5 and N-Q. While for KOH activation, as shown in Table 2, most of the N was released during the process, the N-containing species shown here might be not that representative considering its low content. In general, the differences in carbon defects and O-/N-containing groups for varied biocarbon materials might result in a distinct performance in CO_2 adsorption, as the surface chemical structures could affect its affinity with target molecules.

The changes in carbon skeleton of the biocarbon materials after different treatments were determined by Raman spectrometry, the spectra between 1800 and 800 cm^{-1} were deconvoluted into 10 Gaussian bands using PeakFit v4.12 software with the band assignments shown elsewhere [38]. The resulted ratios of Raman band areas I_D/I_G and $I_D/I_{(GR + VL + VR)}$ of different biocarbon materials are thus shown in Fig. 5. Here, the band ratios of I_D/I_G and $I_D/I_{(GR + VL + VR)}$ represent the ratio of large aromatic ring systems (≥6 fused rings) in the whole aromatic ring systems and the relative ratio of large (≥6 fused rings) and small (3–5 fused rings) aromatic ring systems in the biocarbon materials, respectively.

From Fig. 5, it can be observed that the ratio of I_D/I_G was largely

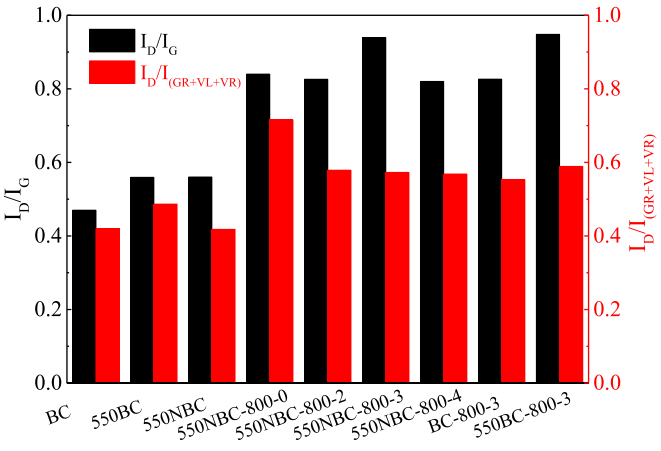


Fig. 5. Ratios of Raman band areas I_D/I_G and $I_D/I_{(GR + VL + VR)}$ of biocarbon materials obtained under different conditions.

dependent on the temperature that biocarbon materials experienced, higher temperature would generally correspond to a higher value of I_D/I_G. For instance, 550BC and 550NBC showed almost the same I_D/I_G value, which was obviously higher that of BC. Similarly, the biocarbon materials experienced 800 °C no matter with/without activation and N-doping and one-/two-step process exhibited higher values of I_D/I_G than those of 550BC and 550NBC. Higher temperature would generate more large aromatic ring systems in biocarbon materials. While for $I_D/I_{(GR + VL + VR)}$, heat treating at 550 °C (550BC) could increase the ratio of large aromatic ring systems to small aromatic ring systems, indicating transformation of small rings to large rings with higher carbonization degree. N-doping (550NBC) would somehow reduce the condensation of small rings to large rings with the decreased $I_D/I_{(GR + VL + VR)}$. Further heating to 800 °C (550NBC-800-0) again increased the $I_D/I_{(GR + VL + VR)}$, while KOH activation at 800 °C comparatively reduced the $I_D/I_{(GR + VL + VR)}$, but it was still higher than that of biocarbon obtained at 550 °C.

3.4. CO_2 adsorption performance of biocarbon materials

The CO_2 adsorption capacity of all the biocarbon materials was tested at 25 °C, and the results are shown in Table 4. Two adsorption results at 1 and 0.15 bars are given, representing the pure CO_2 adsorption and CO_2 adsorption in flue gas, respectively. From the table, it can be clearly seen that before and after KOH activation, the biocarbon materials showed very different CO_2 adsorption performance. Before activation, the CO_2 adsorption capacity was relatively lower, ranging from 0.29 to 2.15 mmol/g at 1 bar and 0.06–0.86 mmol/g at 0.15 bar. The original BC was not a suitable CO_2 adsorbent due to its rare pore structure, through heat treatment at 550 °C, 550BC showed an obvious improvement in the CO_2 adsorption capacity as more pores generated (Table 1). But surprisingly, 550NBC displayed similar CO_2 adsorption capacity with 550BC although it had a very low BET surface area (2.20 m^2/g), indicating N-doping indeed enhanced the CO_2 adsorption on biocarbon materials.

After KOH activation, the biocarbon materials showed significantly higher CO_2 adsorption capacity, mainly ranging from 2.43 to 3.82 mmol/g at 1 bar and 0.43–0.83 mmo1/g at 0.15 bar. Wherein, 550NBC-800-2 showed the highest CO_2 capture capacity of 3.82 mmol/g at 1 bar and 25 °C, which was higher than the results of many N-doping porous carbons reported in literature at the same conditions. For instance, Xu et al. [39] prepared N-doped porous walnut shells carbons using KOH, K_2CO_3 and $ZnCl_2$ and other different activators, a maximum CO_2 adsorption capacity of 3.08 mmol/g was obtained. Li et al. [40] reported that the CO_2 absorption capacity of N-doped activated carbon made from water chestnut shell was 3.61 mmol/g. But it should be also noted that a higher BET surface area is not always corresponding to a higher CO_2 adsorption capacity. The CO_2 adsorption capacity of 550NBC-800-3/-4 was found to be lower than that of 550NBC-800-2. Over-activation resulting in micropores damage and merging might be an important reason, as 550NBC-800-2 showed significantly more micropores despite of its much lower total BET surface area. Similarly, BC-800-3 with more micropore area exhibited higher CO_2 adsorption capacity than 550BC-800-3. Further N-doping (550BC-800-3-550 N) did not improve its CO_2 adsorption capacity. The CO_2 adsorption capacity of biocarbon materials at high CO_2 pressure (1 bar) looks more dependent on its micropore areas, other than its mesopore area and N-doping.

However, different trend was observed for CO_2 adsorption of biocarbon materials at low CO_2 pressure of 0.15 bar. Micropores and N-doping both played important roles on its CO_2 adsorption performance. For instance, 550BC showed identical CO_2 adsorption capacity with 550BC-800-3, and higher capacity than 550NBC-800-4, due to combination of its micropores of 118.11 m^2/g and relatively higher N content of 1.37 wt%. 550NBC with very low BET surface area still showed a CO_2 adsorption capacity of 0.55 mmol/g at 0.15 bar due to its high N content, which was even higher or identical with the biocarbon materials with a high BET surface area. What is more, 550NBC-800-0 displayed the highest CO_2 adsorption capacity of 0.86 mmol/g at 0.15 bar, although 550NBC-800-2 had the highest micropore area and 550BC-800-3-550 N had both high micropore area and enriched N content. A high content of N-5 of 60.29% observed for 550NBC-800-0 in Table 3 might be an important reason, as reported by the literature that N-5 showed a greater capture effect on CO_2 than that of N-6 and N-Q due to the stronger interaction between N-5 and CO_2 molecules [41]. These results indicated that at low CO_2 pressure of 0.15 bar, N-doping, forming more N-5 in biocarbon in particular, might be more important than its micropores.

Table 4
The CO_2 adsorption capacity of different biocarbon materials tested at 25 °C.

Sample	1 bar, mmol/g	0.15 bar, mmol/g
BC	0.29	0.06
550BC	1.57	0.58
550NBC	1.43	0.55
550NBC-800-0	2.15	0.86
550NBC-800-2	3.82	0.83
550NBC-800-3	3.52	0.65
550NBC-800-4	2.43	0.43
BC-800-3	3.41	0.73
550BC-800-3	3.02	0.56
550BC-800-3-550 N	2.98	0.58

4. Conclusion

In this study, N-doped porous biocarbon materials were prepared through co-pyrolysis of biocoke with urea (N-doping) and KOH activation, and their physiochemical structures and CO_2 adsorption capacity were analyzed. The results showed that N-doping at 550 °C would decrease the yield of biocarbon and block its pores compared with direct heat treatment, through further heating to 800 °C, its pore structure could be recovered along with more weight loss. KOH activation could produce highly porous biocarbon materials in the expense of yield reduction. Moderate activation (550NBC-800-2) could generate more micropores, over activation (550NBC-800-3/4) could further increased its total surface area, but resulted in the damage/merging of micropores to mesopores. KOH activation was found to increase the O-containing groups and decrease the large ring systems in the biocarbon as well, but the etching of KOH would lead to the releasing of N previously existed/doped in the biocarbon. The CO_2 adsorption performance of the biocarbon material was closely related to its pore structure and surface N-doping. At a high CO_2 pressure (1 bar), the CO_2 adsorption capacity of biocarbon materials was more dependent on its micropore areas. But at a low CO_2 pressure (0.15 bar), N-doping, especially to form more N-5 in biocarbon, was observed to be more important than its micropores.

CRediT authorship contribution statement

Jiazhen Tang: Writing – original draft, Investigation, Formal analysis, Data curation. **Bin Li:** Writing – review & editing, Writing – original draft, Supervision, Funding acquisition, Formal analysis, Conceptualization. **Yusuf Makarfi Isa:** Writing – review & editing. **Xing Xie:** Writing – review & editing, Supervision, Conceptualization. **Alexander Kozlov:** Writing – review & editing. **Maxim Penzik:** Writing – review & editing. **Dongjing Liu:** Writing – review & editing.

Data availability

Data will be made available on request.

Acknowledgements

The authors would like to express their sincere thanks for the financial support from the National Natural Science Foundation of China

(52276196), the Changzhou Basic Research Program (CJ20220183) and the High-level Talent Foundation of Anhui Agricultural University (rc412307).

References

[1] Y. Wang, B. Li, A. Gao, K. Ding, X. Xing, J. Wei, Y. Huang, J. Chun-Ho Lam, K. A. Subramanian, S. Zhang, Volatile-char interactions during biomass pyrolysis: effect of biomass acid-washing pretreatment, Fuel 340 (2023) 127496.

[2] B. Li, H. Huang, X. Xie, J. Wei, S. Zhang, X. Hu, S. Zhang, D. Liu, Volatile-char interactions during biomass pyrolysis: effects of AAEMs removal and KOH addition in char, Renew. Energy 219 (2023) 119459.

[3] B. Li, M. Song, X. Xie, J. Wei, D. Xu, K. Ding, Y. Huang, S. Zhang, X. Hu, S. Zhang, D. Liu, Oxidative fast pyrolysis of biomass in a quartz tube fluidized bed reactor: effect of oxygen equivalence ratio, Energy 270 (2023) 126987.

[4] B. Li, L. Zhao, X. Xie, D. Lin, H. Xu, S. Wang, Z. Xu, J. Wang, Y. Huang, S. Zhang, X. Hu, D. Liu, Volatile-char interactions during biomass pyrolysis: effect of char preparation temperature, Energy 215 (2021) 119189.

[5] S. Liu, G. Wu, Y. Gao, B. Li, Y. Feng, J. Zhou, X. Hu, Y. Huang, S. Zhang, H. Zhang, Understanding the catalytic upgrading of bio-oil from pine pyrolysis over CO_2-activated biochar, Renew. Energy 174 (2021) 538–546.

[6] S. Zhang, K. Zou, B. Li, H. Shim, Y. Huang, Key considerations on the industrial application of lignocellulosic biomass pyrolysis toward carbon neutrality, Engineering 29 (2023) 35–38.

[7] A.-N. Huang, C.-P. Hsu, B.-R. Hou, H.-P. Kuo, Production and separation of rice husk pyrolysis bio-oils from a fractional distillation column connected fluidized bed reactor, Powder Technol. 323 (2018) 588–593.

[8] H. Wang, Y. Liu, R. Gunawan, L. Zhang, Z. Wang, C.-Z. Li, Reactions and distribution of levoglucosan during the high-pressure reactive distillation of bio-oil, Ind. Eng. Chem. Res. 60 (2021) 6298–6305.

[9] L. Qu, X. Jiang, Z. Zhang, X-g Zhang, G-y Song, H-l Wang, Y-p Yuan, Y-l Chang, A review of hydrodeoxygenation of bio-oil: model compounds, catalysts, and equipment, Green Chem. 23 (2021) 9348–9376.

[10] S.K. Tanneru, P.H. Steele, Direct hydrocracking of oxidized bio-oil to hydrocarbons, Fuel 154 (2015) 268–274.

[11] X. Yuan, M. Sun, C. Wang, X. Zhu, Full temperature range study of rice husk bio-oil distillation: distillation characteristics and product distribution, Separ. Purif. Technol. 263 (2021) 118382.

[12] H. Wang, R. Gunawan, Z. Wang, L. Zhang, Y. Liu, S. Wang, M.D.M. Hasan, C.-Z. Li, High-pressure reactive distillation of bio-oil for reduced polymerisation, Fuel Process. Technol. 211 (2021) 106590.

[13] S. Kadarwati, X. Hu, R. Gunawan, R. Westerhof, M. Gholizadeh, M.D.M. Hasan, C.-Z. Li, Coke formation during the hydrotreatment of bio-oil using NiMo and CoMo catalysts, Fuel Process. Technol. 155 (2017) 261–268.

[14] S. Li, S. Zhang, Z. Feng, Y. Yan, Coke Formation in the catalytic cracking of bio-oil model compounds, Environ. Prog. Sustain. Energy 34 (2015) 240–247.

[15] Y. Li, C. Zhang, Y. Liu, X. Hou, R. Zhang, X. Tang, Coke deposition on Ni/HZSM-5 in bio-oil hydrodeoxygenation processing, Energy Fuel. 29 (2015) 1722–1728.

[16] X. Wang, W. Deng, C.H. Lam, Y. Xiong, Z. Xiong, J. Xu, L. Jiang, S. Su, S. Hu, Y. Wang, J. Xiang, Coke formation and its impacts during electrochemical upgrading of bio-oil, Fuel 306 (2021) 121664.

[17] Y. Wang, D. Mourant, X. Hu, S. Zhang, C. Lievens, C.-Z. Li, Formation of coke during the pyrolysis of bio-oil, Fuel 108 (2013) 439–444.

[18] B. Li, X. Xie, L. Zhang, D. Lin, S. Wang, S. Wang, H. Xu, J. Wang, Y. Huang, S. Zhang, D. Liu, Coke formation during rapid quenching of volatile vapors from fast pyrolysis of cellulose, Fuel 306 (2021) 121658.

[19] L. Wu, X. Hu, S. Wang, D. Mourant, Y. Song, T. Li, C.-Z. Li, Formation of coke during the esterification of pyrolysis bio-oil, RSC Adv. 6 (2016) 86485–86493.

[20] D.C. Elliott, T.R. Hart, G.G. Neuenschwander, L.J. Rotness, M.V. Olarte, A. H. Zacher, Y. Solantausta, Catalytic hydroprocessing of fast pyrolysis bio-oil from pine sawdust, Energy Fuel. 26 (2012) 3891–3896.

[21] D.C. Elliott, T.R. Hart, G.G. Neuenschwander, L.J. Rotness, A.H. Zacher, Catalytic hydroprocessing of biomass fast pyrolysis bio-oil to produce hydrocarbon products, Environ Prog Sustain 28 (2009) 441–449.

[22] H. Shahbeik, A. Shafizadeh, V.K. Gupta, S.S. Lam, H. Rastegari, W. Peng, J. Pan, M. Tabatabaei, M. Aghbashlo, Using nanocatalysts to upgrade pyrolysis bio-oil: a critical review, J. Clean. Prod. 413 (2023) 137473.

[23] Y. Zhang, J. Monnier, M. Ikura, Bio-oil upgrading using dispersed unsupported MoS_2 catalyst, Fuel Process. Technol. 206 (2020) 106403.

[24] X. Hu, Z. Zhang, M. Gholizadeh, S. Zhang, C.H. Lam, Z. Xiong, Y. Wang, Coke Formation during thermal treatment of bio-oil, Energy Fuel. 34 (2020) 7863–7914.

[25] B. Li, J. Tang, H. Huang, X. Xie, D. Lin, S. Zhang, Y. Huang, D. Liu, Z. Xu, D. Chen, Biocoke production from heat treatment of bio-oil: effect of temperature, J. Anal. Appl. Pyrol. 161 (2022) 105401.

[26] G. Huang, X. Wu, Y. Hou, J. Cai, Sustainable porous carbons from garlic peel biowaste and KOH activation with an excellent CO_2 adsorption performance, Biomass Conversion and Biorefinery 10 (2019) 267–276.

[27] D. Tiwari, H. Bhunia, P.K. Bajpai, Adsorption of CO_2 on KOH activated, N-enriched carbon derived from urea formaldehyde resin: kinetics, isotherm and thermodynamic studies, Appl. Surf. Sci. 439 (2018) 760–771.

[28] J. Han, L. Zhang, B. Zhao, L. Qin, Y. Wang, F. Xing, The N-doped activated carbon derived from sugarcane bagasse for CO_2 adsorption, Ind. Crop. Prod. 128 (2019) 290–297.

[29] J. Shi, H. Cui, J. Xu, N. Yan, S. You, Synthesis of N-doped hierarchically ordered micro-mesoporous carbons for CO_2 adsorption, J. CO2 Util. 62 (2022) 102081.

[30] J. Bai, J. Huang, Q. Yu, M. Demir, M. Kilic, B.N. Altay, X. Hu, L. Wang, N-doped porous carbon derived from macadamia nut shell for CO_2 adsorption, Fuel Process. Technol. 249 (2023) 107854.

[31] J. Zhang, H. Chen, J. Bai, M. Xu, C. Luo, L. Yang, L. Bai, D. Wei, W. Wang, H. Yang, N-doped hierarchically porous carbon derived from grape marcs for high-performance supercapacitors, J. Alloys Compd. 854 (2021) 157207.

[32] J. Wang, I. Senkovska, M. Oschatz, M.R. Lohe, L. Borchardt, A. Heerwig, Q. Liu, S. Kaskel, Highly porous nitrogen-doped polyimine-based carbons with adjustable microstructures for CO_2 capture, J. Mater. Chem. A 1 (2013) 10951–10961.

[33] Z-h Tang, Z. Han, G-z Yang, B. Zhao, S-l Shen, J-h Yang, Preparation of nanoporous carbons with hierarchical pore structure for CO_2 capture, N. Carbon Mater. 28 (2013) 55–60.

[34] M. Sevilla, A.B. Fuertes, CO_2 adsorption by activated templated carbons, J. Colloid Interface Sci. 366 (2012) 147–154.

[35] M. Smith, L. Scudiero, J. Espinal, J.-S. McEwen, M. Garcia-Perez, Improving the deconvolution and interpretation of XPS spectra from chars by ab initio calculations, Carbon 110 (2016) 155–171.

[36] B. Li, J. Tang, X. Xie, J. Wei, D. Xu, L. Shi, K. Ding, S. Zhang, X. Hu, S. Zhang, D. Liu, Char structure evolution during molten salt pyrolysis of biomass: effect of temperature, Fuel 331 (2023) 125747.

[37] M. Ayiania, M. Smith, A.J.R. Hensley, L. Scudiero, J.-S. McEwen, M. Garcia-Perez, Deconvoluting the XPS spectra for nitrogen-doped chars: an analysis from first principles, Carbon 162 (2020) 528–544.

[38] X. Li, J-i Hayashi, C.-Z. Li, FT-Raman spectroscopic study of the evolution of char structure during the pyrolysis of a Victorian brown coal, Fuel 85 (2006) 1700–1707.

[39] Y. Xu, Z. Yang, G. Zhang, P. Zhao, Excellent CO_2 adsorption performance of nitrogen-doped waste biocarbon prepared with different activators, J. Clean. Prod. 264 (2020) 121645.

[40] Q. Li, S. Liu, W. Peng, W. Zhu, L. Wang, F. Chen, J. Shao, X. Hu, Preparation of biomass-derived porous carbons by a facile method and application to CO_2 adsorption, J. Taiwan Inst. Chem. Eng. 116 (2020) 128–136.

[41] J. Chen, J. Yang, G. Hu, X. Hu, Z. Li, S. Shen, M. Radosz, M. Fan, Enhanced CO_2 capture capacity of nitrogen-doped biomass-derived porous carbons, ACS Sustain. Chem. Eng. 4 (2016) 1439–1445.